Gamma-ray observations indicate that nuclear interactions between energetic protons and ambient gas occur at various depths in the solar atmosphere, especially those associated with the lower chromosphere or the photosphere (*11*). The gamma-ray observations also indicate that these reactions occur prodigiously; in number, the interacting protons are generally more numerous than those escaping from the Sun (*12*). Preliminary theoretical estimates suggest that the time-averaged solar flare production at the surface of the Sun is on the order of 0.1 $^{10}Be/cm^2 \cdot s$ (*13*). The SW escape rate from the Sun is $\sim 10^{13}$ $H/cm^2 \cdot s$, corresponding to a SW removal rate of 3×10^{26} H/cm^2 per million years. This corresponds to a column depth of gas extending down about 2000 km into the photosphere. If the ^{10}Be produced in the top 10^{24} H/cm^2 of the Sun's atmosphere is not mixed any deeper than 2000 km into the photosphere in a million years, we would expect the SW to carry away the entire ^{10}Be production at the rate of 0.1 $atom/cm^2 \cdot s$. If the ^{10}Be is mixed within that time through the solar convective zone, probably 1 to 2×10^5 km below the photosphere, then the mean ^{10}Be concentration would be diluted by four to five orders of magnitude. Our result suggests that most of the ^{10}Be is ejected in the SW and large flares without mixing and loss into the deeper solar convective zone.

References and Notes

1. X. M. Hua, R. Ramaty, R. E. Lingenfelter, *Astrophys. J.* **341**, 516 (1989).
2. R. V. Morris, R. Score, C. Dardano, G. Heiken, *Handbook of Lunar Soils* (Publication 67, Johnson Space Center, Houston, TX, 1983).
3. J. C. Davis *et al.*, *Nucl. Instrum. Methods Phys. Res. Sect. B* **B52**, 269 (1990).
4. L. A. Rancitelli, R. W. Perkins, W. D. Felix, N. A. Wogman, *Proc. Lunar Sci. Conf.* **5**, 2185 (1974).
5. Y. Langevin, J. R. Arnold, K. Nishiizumi, *J. Geophys. Res.* **87**, 6681 (1982).
6. A. J. T. Jull, D. Lal, L. R. McHargue, G. S. Burr, D. J. Donahue, *Nucl. Instrum. Methods Phys. Res. Sect. B* **B172**, 867 (2000).
7. F. Begemann, W. Born, H. Palme, E. Vilcsek, H. Wänke, *Proc. Lunar Sci. Conf.* **3**, 1693 (1972).
8. E. L. Fireman, J. DeFelice, J. D'Amico, *Proc. Lunar Sci. Conf.* **8**, 3749 (1977).
9. A. J. T. Jull, D. Lal, D. J. Donahue, *Earth Planet. Sci. Lett.* **136**, 693 (1995).
10. J. F. Ziegler, J. P. Biersack, U. Littmark, *The Stopping and Range of Ions in Solids* (Pergamon, New York, 1985).
11. R. Ramaty, J. A. Miller, X.-M. Hua, R. E. Lingenfelter, *Astrophys. J. Suppl.* **73**, 199 (1990).
12. R. J. Murphy, R. Ramaty, *Adv. Space Res.* **4**, 127 (1984).
13. R. E. Lingenfelter, R. Ramaty, personal communication.

14. The authors wish to thank R. E. Lingenfelter for stimulating discussion and suggestion. This work was originated by discussion with J. R. Arnold who kindly supported the project. This work was supported by NASA grants NAG5-4992 and NAG9-1051. A part of this work was performed under the auspices the U.S. Department of Energy by University of California Lawrence Livermore National Laboratory under contract W-7405-Eng-48.

15 May 2001: accepted 5 September 2001

Seismic Observations of Splitting of the Mid–Transition Zone Discontinuity in Earth's Mantle

Arwen Deuss* and John Woodhouse

The transition zone of Earth's mantle is delineated by globally observed discontinuities in seismic properties at depths of about 410 and 660 kilometers. Here, we investigate the detailed structure between 410 and 660 kilometers depth, by making use of regional stacks of precursors to the SS phase. The previously observed discontinuity at about 520 kilometers depth is confirmed in many regions, but is found to be absent in others. There are a number of regions in which we find two discontinuities at about 500 and 560 kilometers depth, an effect which can be interpreted as a "splitting" of the 520 kilometer discontinuity. These observations provide seismic constraints on the sharpness and observability of mineralogical phase transitions in the mantle transition zone.

The characteristics of the mantle transition zone (between 410 and 660 km) are important for our understanding of Earth's dynamics. Constraints on seismic velocity discontinuities in the transition zone can be obtained from reflection observations of seismic waves and high-pressure experiments on mantle rocks. The 410-km discontinuity is generally thought to be caused by the phase transformation of low-pressure olivine (α-phase) to wadsleyite (β-phase) and the 660-km discontinuity by the phase transformation of ringwoodite (γ-phase) to perovskite and magnesiowüstite (*1, 2*). Over the past decades, a number of seismic studies have demonstrated the global existence of these discontinuities and have mapped their topography (*3–6*).

A number of studies have reported a weaker discontinuity, in the mid–transition zone, at about 520-km depth. The 520-km discontinuity is generally believed to be caused by the transition in the mantle olivine component from wadsleyite (β-phase) to ringwoodite (γ-phase) (*1, 7*); the Clapeyron slope of this transition is 4 MPa K^{-1}. The most consistent seismic evidence for the 520-km discontinuity comes from long-period S wave observations using SS precursors (*5, 6, 8, 9*) or ScS reverberations (*10*). Some studies claim that the 520-km discontinuity is a global feature (*8, 9*), whereas others find that it can be observed only in certain regions (*5*) or that it is not found beneath continental shields (*6*). It is much more difficult to observe reflections from this discontinuity in short-period data (*11*), and refracted wave studies (*12, 13*) do not find evidence for a discontinuity at 520 km, suggesting that it is not a sharp reflector, but a velocity gradient with a wide transition interval (*14*).

We investigate the characteristics of the 520-km discontinuity in detail by using precursors to the SS phase, which are underside reflections at a discontinuity below the SS bounce point. Long-period SS waves are used to investigate properties of the 520-km discontinuity, because they are sensitive to weak discontinuities. The precursors have small amplitudes and cannot be observed in individual seismograms. Thus, we stack the traces in the slowness-time domain to suppress incoherent noise and to enhance the visibility of the precursors. Such stacks amplify and clarify the peaks in amplitude associated with the major discontinuities at 410 and 660 km and provide a means of investigating hypotheses about the existence and regional variation of the weaker 520-km discontinuity.

We use a global data set of 7018 seismograms collected from the Incorporated Research Institutions for Seismology/International Deployment of Accelerometers (IRIS/IDA) global network (*15*); this is the type of data set that has been used in other studies to obtain global maps of topography on transition zone discontinuities. A stack of all seismograms in our data set shows reflections from "410" and "660" and a weaker reflection from a depth of about 520 km (Fig. 1).

We divide Earth's surface into 407 spherical caps with 10° radius (*16*) and stack all seismograms with bounce points in each cap. North America and the north Pacific provide an excellent region to observe small-scale regional variations in the 520-km discontinuity, because it is well covered by SS wave bounce points. The North American cross

Department of Earth Sciences, University of Oxford, Oxford OX1 3PR, UK.

*To whom correspondence should be addressed. E-mail: arwen.deuss@earth.ox.ac.uk

sections go from the tectonically active west to the stable shield in the east. In the mid-Pacific, all except for three traces show one relatively clear reflection from a depth of around 520 km. In nine traces for North America—in particular, below the shield region in the east—there are two equally large reflections from depths of about 506 and 562 km (Fig. 1). In three traces in the east Pacific, a small secondary arrival can be seen arriving next to the much larger first arrival.

Double reflections from 500 to 515 km and 551- to 566-km depth are also found in the Indonesian subduction zone and the North African shield (Fig. 2). However, the South American shield and the Indian shield show a single reflector at 530 km. The Pacific also shows a single reflector from 530-km depth, but there are no clear reflections close to the equator in this section, although the stacks contain more than 100 traces each.

We have used a bootstrap resampling algorithm (*17*) to determine the robustness of the splitting observations. Examples of resampled stacks and 95% confidence levels are provided as supplementary material (*18*). We also refiltered the data in shorter and longer period bands. For shorter periods, the two peaks are more pronounced (Fig. 3). For longer period filtering, the two split peaks become less distinguishable, and this might explain why previous long-period shear wave studies find only one reflector.

The global observations of single and split reflections of the mid–transition zone discontinuity show a complex structure (Fig. 4). We have employed a cross-correlation technique (*19*) to decide on the type of reflection (single or double), and additionally, checked the result by visual inspection. There is no obvious correlation (*20*) between the characteristics of the 520-km discontinuity and surface tectonics, as suggested by others (*5, 6*). However, there are substantial regional variations in depth and observability, and these can be compared with fast/cold regions versus slow/hot regions in tomographic models. The cold subduction zone region of the west Pacific and Indonesia, and also the seismically fast region in west Africa show double reflections, but double reflections also appear in slow regions, for example, close to Greenland, in the Atlantic Ocean, and in the mid-Pacific. The earlier inference (*6*) that the 520-km discontinuity was not found when data were stacked for shield regions may result from the fact that its character is variable beneath different shield regions. For example, the double reflections beneath the North American and African shields and the single reflections beneath other shield regions could lead to a null result when all shield data are combined in a single stack.

We seek an explanation for splitting of the mid–transition zone discontinuity from mineral physics. Apart from the transition in the mantle olivine component from wadsleyite (β-phase) to ringwoodite (γ-phase), the nonolivine components should also be taken into account for a pyrolite composition of the mantle. It has recently been shown that the nonolivine component is important for the 660-km discontinuity; the addition of a transformation to garnet explains multiple reflections from the base of the transition zone

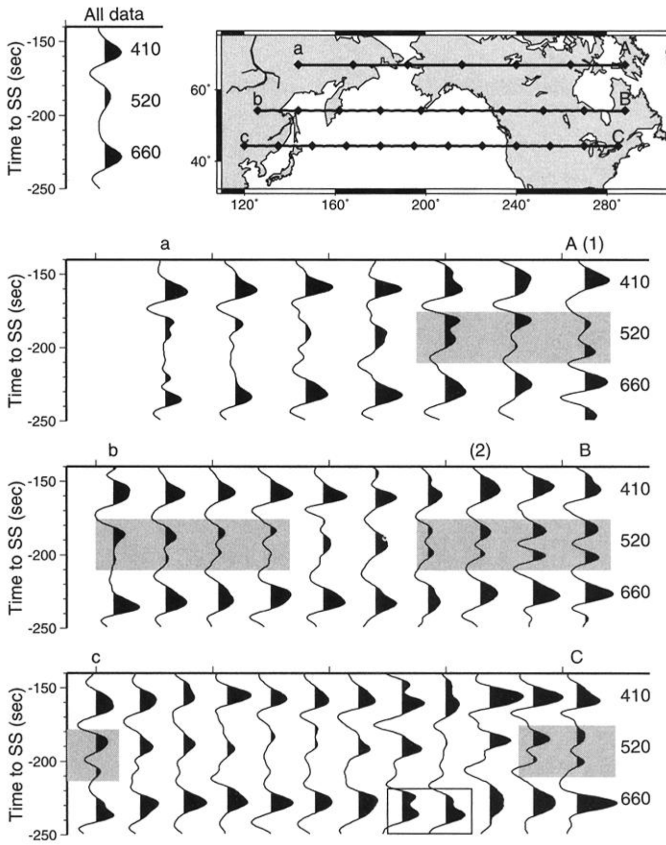

Fig. 1. Stacked traces for an east-west cross section through North America. On average, 160 seismograms are stacked in one trace. The traces show peaks in amplitude related to reflections from the major discontinuities at about 410 and 660 km. Between the "410" and "660" arrivals, there are signals from a range of depths; all traces with two reflections are marked (gray boxes). Note the multiple arrivals from "660" in cross section cC (white box), confirm earlier observations of multiple discontinuities in this region (*21*). Numbers (1) and (2) above the traces indicate the traces shown in Fig. 3.

Fig. 2. Global observations of the 520-km discontinuity. The cross sections are computed using the same data set as in Fig. 1.

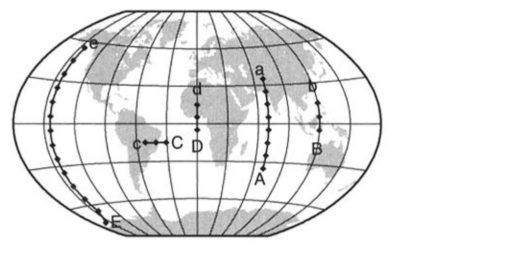

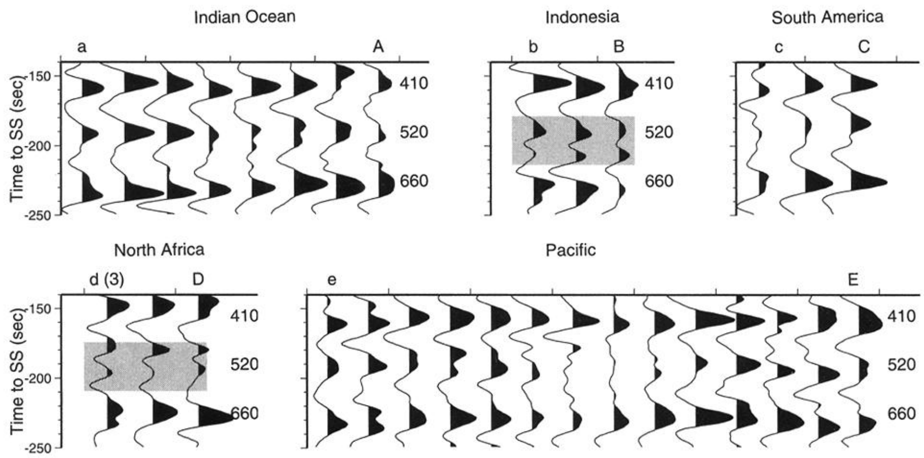

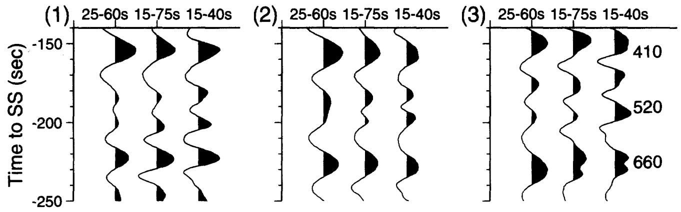

Fig. 3. Stacks refiltered in different period bands; the examples correspond to the numbered stacks in Figs. 1 and 2. For shorter periods (15 to 40 s), the two split peaks become sharper; for longer periods (25 to 60 s), the two peaks become less sharp and for stack (2) even indistinguishable.

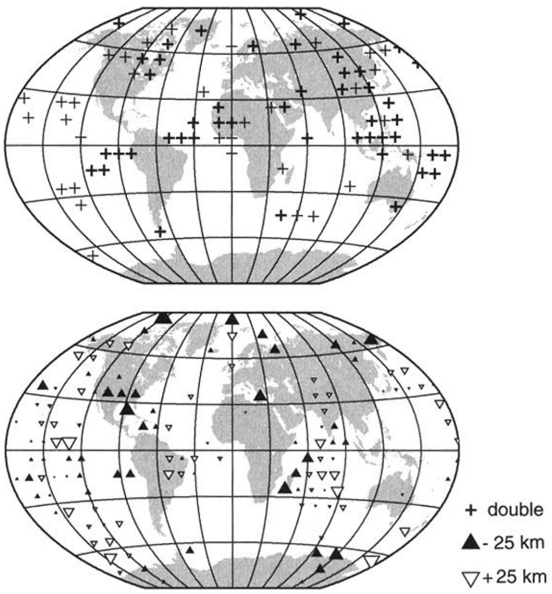

Fig. 4. Global observations of single reflections and splitting of the mid–transition zone discontinuity. Double reflections determined using the cross-correlation technique are marked with a bold plus. Weaker double reflections (obtained by visual inspection) are also shown. In the case of a single reflection, the topography on the mid–transition zone discontinuity is determined and plotted as deviation from the average depth of 525 km. The topography measurements are corrected for crustal (*31*) and mantle (*25*) structure.

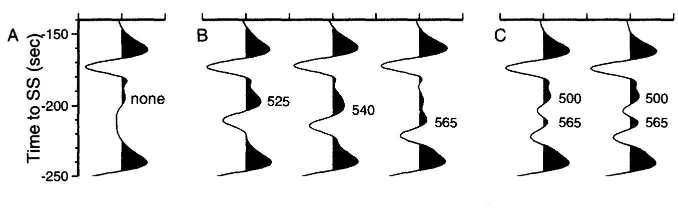

Fig. 5. Synthetic seismograms computed with WKBJ ray tracing (*32*). (**A**) No mid–transition zone discontinuity. (**B**) One mid–transition zone discontinuity with an impedance contrast of 4.8% [i.e., the total contribution of the garnet and olivine transition (*30*)] at depths of 525, 540, and 565 km. (**C**) Split mid–transition zone discontinuity with the impedance contrast from mineralogy (1.66% and 3.13%) and one with slightly larger impedance contrasts of 2.4% and 4.3%.

(*21*), a feature which can also be seen in our data (Fig. 1). A transformation of garnet to Ca-rich perovskite occurs in the mid–transition zone with a Clapeyron slope of 0 to –2 MPa K^{-1} (*2, 22, 23*). This transformation may be an important contributor to the 520-km discontinuity as well as to continuous changes in transition zone mineralogy through to the 670-km discontinuity (*24*).

If both transformations contribute to the characteristics of the 520-km discontinuity, then this could result either in two separate reflectors or one single reflector, depending on composition and temperature. Using the data summarized by Ita and Stixrude (*2*), and assuming that the two components do not interact chemically, we find that these two transformations will appear at the same depth for an average mantle temperature of 1500 K. In this case, a single reflection would be observed. Because both transitions are sensitive to temperature, the transitions will move to a different depth for locally higher or lower temperature and result into two discontinuities.

Correlations with tomographic models (*25*) indicate, however, that the depth variations that we observed are not well explained by temperature variations alone. We infer that the observed variations must be an effect dependent upon both temperature and composition. For example, local variations in minor phases containing Fe and Ca would have an effect on the location and visibility of the boundaries; Fe-partitioning between the garnet and the β- and γ-phases of $(Mg,Fe)_2SiO_4$ could reduce the transition width, rendering both transformations seismically observable (*24*). The β-γ transition is also sensitive to Mg/(Mg+Fe) (*26*) and does not occur if the Fe content is too high. If the Ca content of the garnet is too low, there will be no pseudo–first-order transition to Ca-perovskite (*24*). Other trace components—for example, water—would change the sharpness of the β-γ transition (*27, 28*). Thus, a single reflection could correspond to Ca-poor regions, high Fe content, or dry mantle conditions.

To illustrate the seismological effects of such a single or double discontinuity, we compute synthetic seismograms for the Preliminary Reference Earth Model (*29*), modified to contain one or two discontinuities in the mid–transition zone (*30*), and compare them with the observations. The synthetic without a 520-km discontinuity (Fig. 5) shows a small side-lobe of the 410-km discontinuity, but the amplitude is much smaller than the observations for the mid–transition zone discontinuity. The models with one discontinuity are similar to observations with one reflection. The side-lobe of 410 produces a small secondary peak, but the amplitude of this secondary arrival is much smaller than our splitting observations, and it does not result in two separate peaks. Note that for a depth of 565 km, the signal becomes very broad and is similar to the small amplitudes we observed in the Pacific near the equator (Fig. 2E). Only the models with two discontinuities can produce the two separate peaks that we observe for the "split" observations and match the splitting observations as seen, for example, in Indonesia (Fig. 2B).

Our data show the regional occurence of either a single reflector at around 520 km or two reflectors at 500- and 560-km depth; this can be used as a probe for composition in the mantle transition zone. The substantial regional variation in depth and observability of the 520-km discontinuity shows that the mantle transition zone is less homogeneous than is generally assumed.

References and notes

1. A. E. Ringwood, *Composition and Petrology of the Earth's Mantle* (McGraw-Hill, New York, 1975).
2. J. Ita, L. Stixrude, *J. Geophys. Res.* **97**, 6849 (1992).
3. P. M. Shearer, G. Masters, *Nature* **355**, 791 (1992).
4. M. P. Flanagan, P. M. Shearer, *J. Geophys. Res.* **103**, 2673 (1998).
5. J. Gossler, R. Kind, *Earth Planet. Sci. Lett.* **138**, 1 (1996).
6. Y. Gu, A. M. Dziewonski, C. B. Agee, *Earth Planet. Sci. Lett.* **157**, 57 (1998).
7. S. M. Rigden, G. D. Gabriel, J. D. F. Gerald, I. Jackson, R. C. Liebermann, *Nature* **345**, 143 (1991).
8. P. M. Shearer, *Nature* **344**, 121 (1990).
9. ———, *J. Geophys. Res.* **101**, 3053 (1996).
10. J. Revenaugh, T. H. Jordan, *J. Geophys. Res.* **96**, 19736 (1991). The ScS phase in the reflection of S-waves from the core-mantle boundary.
11. Ryberg, F. Wenzel, A. V. Egorkin, L. Solodilov, *J. Geophys. Res.* **102**, 5413 (1997).
12. L. E. Jones, J. Mori, D. V. Helmberger, *J. Geophys. Res.* **97**, 8765 (1992).

13. P. R. Cummins, B. L. N. Kennet, J. R. Bowman, M. G. Bostock, *Bull. Seismol. Soc. Am.* **82**, 323 (1992).
14. H. M. Benz, J. E. Vidale, *Nature* **365**, 147 (1993).
15. We included 1530 events with a depth from 0 to 75 km, a magnitude of $6.0 \leq M_w \leq 7.0$, and from stations in the epicentral distance range $100° \leq \Delta \leq 160°$ for the period 1 January 1980 to 29 March 1998. The SS phases in the individual traces are hand-picked, and the data is deconvolved for receiver effects and bandpass-filtered between 15 and 75 s.
16. The size of the caps corresponds to the Fresnel zone of the SS rays. Neighboring caps overlap partly to ensure smoothing.
17. B. Efron, R. Tibshirani, *Science* **253**, 390 (1991). The data set was also divided into two subsets with epicentral distances from 100° to 130° and 130° to 160°; splitting was still present in stacks of the subsets.
18. Supplementary material is available at www.sciencemag.org/cgi/content/full/294/5541/354/DC1
19. The stacks are cross-correlated with the SS pulse; splitting is determined by two cross-correlation maxima (instead of one) in the depth range of 480 to 600 km.
20. We find single reflections from 520 km for stacks corresponding to different regional types (shields, tectonically active regions, stable continents, and oceans). The stacks exhibit somewhat different amplitudes and, in particular, the shield stack shows a smaller amplitude, confirming an earlier study (*6*).
21. N. A. Simmons, H. Gurrola, *Nature* **405**, 559 (2000).
22. D. Canil, *Phys. Earth Planet. Inter.* **86**, 25 (1994).
23. S. Koito, M. Akaogi, O. Kubuta, T. Suzuki, *Phys. Earth Planet. Inter.* **120**, 1 (2000).
24. D. J. Weidner, Y. Wang, in *Earth's Deep Interior: Mineral Physics and Tomography from the Atomic to the Global Scale* (Geophysical Monograph 117, American Geophysical Union, Washington, DC, 2000), pp. 215–235.
25. J. Ritsema, H. J. van Heijst, J. H. Woodhouse, *Science* **286**, 1925 (1999).
26. Y. Fei, C. Bertka, in *Mantle Petrology: Field Observations and High-Pressure Experimentation*, Special Publication in honor of Francis R. Boyd, *Geochem. Soc. Spec. Pub.* (Geochemical Society, Washington University, St. Louis, MO, 1999), vol. 6, pp. 189–207.
27. T. Inoue, D. J. Weidner, P. A. Northrup, J. B. Parise, *Earth Planet. Sci. Lett.* **160**, 107 (1998).
28. H. Yusa, T. Inoue, Y. Ohishi, *Geophys. Res. Lett.* **27**, 413 (2000).
29. A. Dziewonski, D. Anderson, *Phys. Earth Planet. Inter.* **25**, 297 (1981).
30. Previous SS-precursor studies suggest a shear wave impedance contrast of 6 to 10% for the 410-km discontinuity and 10% for the 660-km discontinuity (9). In the mid–transition zone region, computer simulations for a pyrolite mantle composition give a jump of 1.66% in shear wave impedance for the garnet transition and 3.13% for the olivine transition of the β-phase to γ-phase (*24*).
31. W. D. Mooney, G. Laske, G. Masters, *Eos (Fall Suppl.)* **76**, F421 (1995).
32. C. H. Chapman, *Geophys. Res. Lett.* **3**, 153 (1976). The synthetics are basically delta pulses computed using WKBJ ray tracing for PREM (including attenuation from PREM) and then filtered in the same way as the data.
33. We thank A. Jephcoat and A. Kleppe for useful discussions on mineralogical phase transitions. A.D. was funded by a Scatcherd Scholarship from Oxford University. We also acknowledge support under U.K. Natural Environment Research Council grant GR11534.

18 June 2001; accepted 24 August 2001

An Ossified Meckel's Cartilage in Two Cretaceous Mammals and Origin of the Mammalian Middle Ear

Yuanqing Wang,[1]* Yaoming Hu,[1,2,3] Jin Meng,[2]* Chuankui Li[1]

An ossified Meckel's cartilage has been recovered from two early Cretaceous mammals from China. This element is similar to Meckel's cartilage in prenatal and some postnatal extant mammals and indicates the relationship of Meckel's cartilage with the middle ear in early mammals. The evidence shows that brain expansion may not be the initial factor that caused the separation of postdentary bones from the dentary as middle ear ossicles during mammalian evolution. The failure of the dentary to seize reduced postdentary elements during ontogeny of early mammals is postulated as an alternative mechanism for the separation. Modifications of both feeding and hearing apparatuses in early mammals may have led to the development of the definitive mammalian middle ear.

In nonmammalian vertebrates with jaws, the craniomandibular joint is between the quadrate region of the palatoquadrate and the articular region of Meckel's cartilage (or its replacement). In unequivocal mammals (*1, 2*), the joint is between the squamosal and the dentary. The definitive mammalian middle ear (DMME) is formed by transference of accessory jaw elements, including the angular, articular plus prearticular, and quadrate, to the cranium of mammals as strictly auditory ossicles (renamed as the tympanic, malleus, and incus) (*3*). This transference is one of the central topics of comparative anatomy and evolutionary biology of vertebrates (*3–8*). Although developmental studies of extant mammals have long demonstrated homologies of these elements among jawed vertebrates (*9, 10*), the only fossil evidence on this critical transference is the presence of persistent grooves on the medial surface of the dentary bone, which may have lodged the anterior end of the postdentary unit (PDU, consisting of the endochondral articular and dermal prearticular, angular, and surangular) in some early mammals (*3*).

Four nearly complete *Repenomamus* adult skulls with articulated lower jaws (*11*) and one with articulated lower jaws of an unnamed *Gobiconodon* species (Figs. 1 and 2) were discovered from the Yixian Formation of the lower Cretaceous in Liaoning, China (*12*). Of the two taxa, *Repenomamus* (*11*) represents one of the largest Mesozoic mammals, and is most closely related to gobiconodontids (*13–15*) in sharing basic structures of jaws, teeth, occlusal pattern, and some cranial features (Figs. 1 to 3). Gobiconodontids are related to triconodontids within triconodonts, a diverse grade of basal mammaliaform groups with uncertain relationships (*2, 15–18*) (Fig. 3). Among these specimens, a structure that we recognize as an ossified Meckel's cartilage (OMC) was preserved in two skulls of *Repenomamus* (IVPP specimens V12549 and V12728) and one skull of *Gobiconodon* (IVPP V12585). Of the two OMCs in *Repenomamus*, the one in V12549 is in its original location (Figs. 1, A to C, and 2, A and C), whereas the other in V12728 is displaced and lies between the mandible and the skull (Figs. 1D and 2B). The OMC is rod-like, with a pointed anterior tip and a flared posterior end. It measures 33 mm long in V12549 and 40 mm in V12728. The anterior portion of the OMC in V12549 is lodged in a depression that appears to be an expanded posterior portion of the meckelian groove. The OMC-dentary contact may have had some mobility. During preparation, the OMC was separated from the dentary. In all lower jaws of *Repenomamus*, the anterior tip of the meckelian groove is below m3 (the third lower molariform tooth) and continues anteriorly as a slit that parallels the course of the mandibular canal within the dentary. The mandibular canal, as revealed by radiographic imaging, is low in position, ventral to the long roots of the check teeth, and extends anteriorly to the symphysis. The radiograph shows that in lateral view, the mandibular canal turns slightly dorsally at the position where the anterior tip of the OMC is situated, and extends posteriorly to the mandibular

[1]Institute of Vertebrate Paleontology and Paleoanthropology (IVPP), Chinese Academy of Sciences, Post Office Box 643, Beijing, 100044, China. [2]Division of Paleontology, American Museum of Natural History (AMNH), Central Park West at 79th Street, New York, NY 10024, USA. [3]Biology Program (Ecology, Evolutionary Biology, and Behavior), Graduate School and City College, City University of New York, NY 10016–4309, USA.

*To whom correspondence should be addressed. E-mail: wang.yuanqing@pa.ivpp.ac.cn (Y.W.); jmeng@amnh.org (J.M.)